

## DEVELOPMENT OF CFD MODELS OF MINERAL FLOTATION CELLS

P.T.L. KOH<sup>1</sup>, M.P. SCHWARZ<sup>1</sup>, Y. ZHU<sup>2</sup>, P. BOURKE<sup>3</sup>,  
R. PEAKER<sup>4</sup> and J.P. FRANZIDIS<sup>5</sup>

<sup>1</sup> CSIRO Minerals, Clayton, Victoria 3169, AUSTRALIA

<sup>2</sup> CSIRO Manufacturing and Infrastructure Technology, Highett, Victoria 3190, AUSTRALIA

<sup>3</sup> Outokumpu Technology, West Perth, WA 6005, AUSTRALIA

<sup>4</sup> Metso Minerals, Leatherhead, Surrey KT22 7AX, ENGLAND

<sup>5</sup> JKMRC, Indooroopilly, Queensland 4068, AUSTRALIA

### ABSTRACT

Work in the AMIRA P9M project involves developing Computational Fluid Dynamic (CFD) models of commercial flotation cells used in the mineral processing industry. CFD models provide detailed understanding of the hydrodynamics of flotation cells and are very useful for progressing knowledge of the flotation process and improving operations. Comparisons of the CFD predictions against measured velocities show very good agreement without using any fitting parameter.

### NOMENCLATURE

|            |  |
|------------|--|
| g          | gravity vector [m/s <sup>2</sup> ]                         |
| k          | turbulent kinetic energy [m <sup>2</sup> /s <sup>2</sup> ] |
| P          | pressure [Pa]  |
| U          | velocity vector [m/s]                                      |
| $\epsilon$ | turbulent eddy dissipation [s <sup>-1</sup> ]              |
| $\rho$     | density [kg/m <sup>3</sup> ]                               |
| $\mu$      | dynamic viscosity [Pa-s]                                   |
| $\tau$     | stress tensor [Pa]   |

### INTRODUCTION

One of the objectives of the AMIRA P9M (P780) project is to study the detailed hydrodynamics of flotation cells. As part of its participation in the project, CSIRO has been contracted to develop CFD models of flotation cell hydrodynamics and to validate the models by laboratory measurements.

#### Flotation in Mineral Processing

Flotation is an important and well-established process in the minerals industry. The fundamentals of flotation are however not as well understood as those of other unit operations in this industry. Principles of flotation cell design and operation are mostly empirically based.

Most flotation is carried out using mechanically agitated cells, which are large tanks, ranging in volume up to 150 m<sup>3</sup>, used to separate particles containing valuable minerals from the ore primarily containing gangue. The ground ore is fed into the tanks as slurries as shown in **Figure 1**.

Separation is usually effected by arranging for particles containing valuable minerals to preferentially attach to air bubbles, and hence to be floated to the surface of the slurry via a froth layer, where the particles are removed from the tank by means of an overflow launder. The remainder of the slurry exits the tank through an outlet in the lower part of the cell.

The dispersion of fine air bubbles needed for the flotation is generated by a rotor-stator mechanism, which also serves to mix the slurry and air bubbles. Various different proprietary mechanisms are used in the mineral processing industry. Further details on the principles and practice of mineral flotation can be found in mineral processing books (eg. Wills, 1992).

Metallurgical performance is measured in terms of the rate of flotation of the mineral (recovery), the level of purity of the concentrate (grade) and the level of valuable mineral left in the tailings. Performance is affected by design features such as impeller and stator design, and tank geometry and internals. Flotation is also affected by operating variables such as slurry concentration, aeration rate and impeller speed.

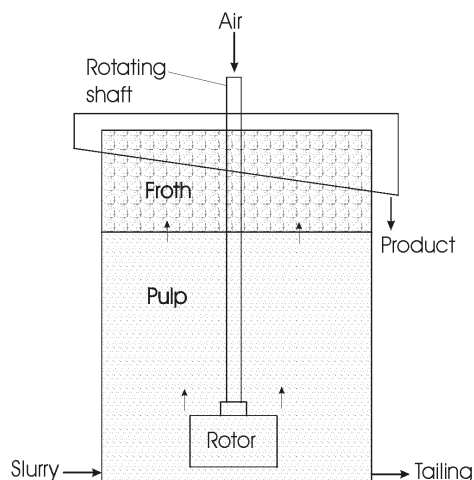


**Figure 1:** Principles of froth flotation.

The CFD technology for the numerical modelling of the complex unsteady, multi-phase flows typically found in agitated tanks of this type has developed to the point where it now has the potential to identify design and operational modifications to the process which can lead to process improvements.

CSIRO Division of Minerals has successfully applied CFD to mineral processes with complex unsteady multi-phase flows. For example, the mixing flow patterns in thickener feedwells have been numerically modelled to locate best positions for flocculant sparge and the results have been successfully implemented in plant equipment.

### Modelling Flotation Cells

In the AMIRA project, two commercial flotation cells have been studied - one fitted with a Metso Minerals flotation mechanism and the other fitted with an Outokumpu flotation mechanism. Physical modelling of the cells was conducted in the CSIRO Thermal and Fluids Engineering laboratory at Highett, while CFD modelling of the flotation cells was performed at CSIRO Minerals at Clayton. The velocity field of the liquid phase was measured using Laser Doppler Velocimetry (LDV). A study of the gas dispersion and residence time distribution in the flotation cells is also an integral part of this work.

CFD models provide detailed understanding of the hydrodynamics of flotation cells and are very useful for progressing knowledge of the flotation process and improving operations. Previous work at CSIRO Minerals in modelling a laboratory-scale Denver flotation cell (Koh *et al.*, 2000) already demonstrated some of the potential for CFD models including better understanding of bubble-particle collisions.

At CSIRO Minerals, we have investigated differences in the metallurgical performances obtained in laboratory tests and during plant trials. The flotation rates in laboratory cells are generally faster in comparison to the flotation rates observed in plant-scale cells. This problem can potentially be solved with the detailed understanding gained from CFD simulations (Koh and Schwarz, 2003).

The observed flotation rates include many effects such as bubble-particle collisions, attachments, detachments, transport times for bubble-particle aggregates to move to the froth layer and transport times within the froth layer. The transport times can be quite significant especially in plant-scale flotation cells as the bubble-particle aggregates have to move over large distances. This may be one of the reasons why flotation rates are much better in laboratory cells where the bubble-particle aggregates have much shorter distances to reach the froth layer.

For practical application, we want to develop a CFD model that does not require extremely long and costly computations that are associated with extremely fine grids, and yet produces sufficiently accurate results. The model needs to be fully three-dimensional (3-D) (ie. 360°) to enable inflows and outflows, as occur in most industrial flotation cells, to be investigated. Importantly, a fully 3-D model allows residence time distributions and flotation kinetics to be calculated within the CFD model. This type of calculation can only be performed in fully 3-D models.

The work presented in this paper is for single-phase flow though the models have been extended to multiple phases as is required to study the flotation process. Such multi-phase simulations are more compute intensive so it is not

possible to use an extremely fine grid because of run time and memory storage limitations. A compromise between the accuracy and the convenience of obtaining results is required so that useful solutions can be obtained fairly quickly.

### MODEL DESCRIPTION

In the simulation of flotation cells, equations for the conservation of mass, momentum and turbulence quantities have been solved. The variables solved include Cartesian velocity components, pressure and turbulence quantities using the continuity and Navier-Stokes equations:

$$\frac{\partial \rho}{\partial t} + \nabla \cdot (\rho \bar{\mathbf{U}}) = 0 \quad (1)$$

$$\frac{\partial (\rho \bar{\mathbf{U}})}{\partial t} + \nabla \cdot (\rho \bar{\mathbf{U}} \otimes \bar{\mathbf{U}}) = -\nabla P + \nabla \cdot (\bar{\boldsymbol{\tau}}) + \rho \bar{\mathbf{g}} \quad (2)$$

Since the flow is in the turbulent regime, the quantities in the above equations are the Reynolds-averaged quantities, and  $\bar{\boldsymbol{\tau}}$  is the effective turbulent stress tensor. By applying the eddy viscosity hypothesis, the Reynolds stresses can be linearly related to the mean velocity gradients in a manner analogous to the relationship between the stress and strain tensors in laminar Newtonian flow:

$$\nabla \cdot (\bar{\boldsymbol{\tau}}) = \nabla \cdot (\mu_{\text{eff}} (\nabla \bar{\mathbf{U}} + (\nabla \bar{\mathbf{U}})^T)) \quad (3)$$

where the effective viscosity is sum of the laminar and turbulent viscosities:

$$\mu_{\text{eff}} = \mu_L + \mu_T \quad (4)$$

The turbulent viscosity in the liquid phase is calculated using the standard  $k$ - $\varepsilon$  turbulence model (Launder and Spalding, 1974):

$$\mu_T = C_\mu \rho \frac{k^2}{\varepsilon} \quad (5)$$

Turbulence kinetic energy  $k$  and turbulence dissipation rate  $\varepsilon$  are solved based on for the liquid phase velocity field. In the present simulation of the liquid phase, the liquid surface is assumed to be flat and frothless.

Two techniques, the sliding-mesh technique and the multiple frames of reference technique, have been used for modelling the impeller rotation in the stationary tank. Time steps corresponding to 15° rotation of the impeller are applied in the sliding mesh technique. The transport equations are solved using the computational fluid dynamics code CFX-4.4 (2001).

For comparison purposes, the Cartesian velocities obtained from the multiple frames of reference technique are converted into cylindrical components  $U_r$ ,  $U_\theta$  and  $U_z$  for the radial, tangential and axial directions respectively.

### EXPERIMENTAL METHOD

The two flotation mechanisms modelled have been supplied by Metso Minerals and by Outokumpu Technology. Both mechanisms were specially manufactured to fit into a large mixing vessel with a

diameter of 1.07 m as shown in **Figure 2**. The volume of liquid in the cell is about 0.8 m<sup>3</sup>.

Time series of velocity were measured in the model cells using an optical fibre LDV system. The transmitting and receiving optics of this probe were mounted on an industrial robotic arm, allowing the probe to be automatically positioned within the tank. Because of the irregular sampling nature of the LDV method, bias correction had to be used to calculate time-mean statistics. The time-mean velocity data thus obtained was found repeatable to within 1%. Time-mean statistics of the velocity data were obtained using a time-weighted bias correction method. The time-mean velocity and turbulent fluctuation were measured point-by-point. The sampling duration was about 4 minutes. The flow field was measured by LDV in the liquid phase without solids and air sparging.



**Figure 2:** Research vessel shown with LDV head manipulated by robot arm for fluid velocity measurement.

## RESULTS

CFD results and the predicted velocities in the liquid phase are discussed separately for the two flotation cells.

### Metso Minerals Flotation Cell

The CFD mesh of the Metso Minerals flotation mechanism has 156,820 grid points as shown in **Figure 3**. It was operated with an impeller speed of 596 rpm with the resulting fluid pressure and flow pattern as indicated in **Figure 4** and **Figure 5**.

The impeller generates a jet stream in the radial direction. Three vortices can be observed in **Figure 5** - one vortex below the impeller, another below the horizontal baffle and a third vortex near the surface. The flow circulates back to the impeller through the top and bottom opening of the stator.

Comparisons have been made between the measured and predicted mean velocity components  $U_r$ ,  $U_\theta$  and  $U_z$  for the radial, tangential and axial directions respectively. Generally, the agreement is very good between the measured and predicted velocities.

The pumping rate of the impeller can be estimated from the radial velocity component and is the highest at the impeller level. Integration of the velocity in the impeller region gives a pumping rate obtained from CFD results which is within 4% of the measured value.

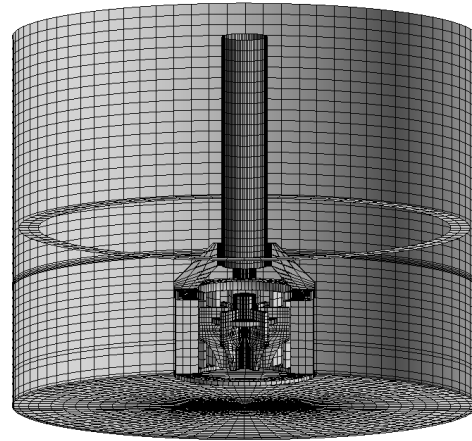


**Figure 3:** Surface grid of Metso Minerals flotation cell.

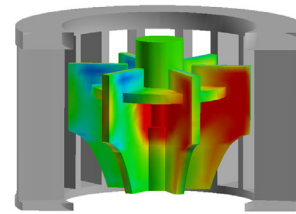


**Figure 4:** Metso Minerals flotation mechanism coloured by fluid pressure.

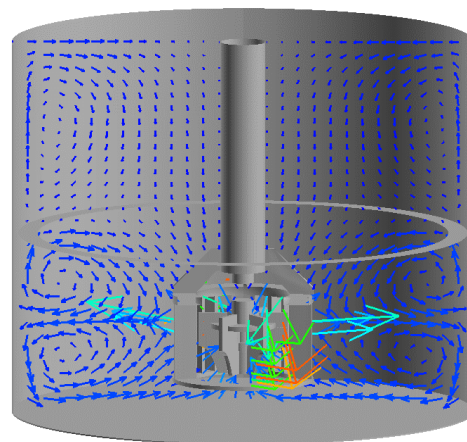


**Figure 5:** CFD predicted velocity vectors in a vertical plane in the Metso Minerals cell.

### Outokumpu Flotation Cell

The Outokumpu impeller was operated at a speed of 328 rpm. The CFD mesh has 146,912 grid points as shown in **Figure 6** with details of the surface grid on the impeller shown in **Figure 7**.

The velocity vectors predicted by CFD in a vertical plane are shown in **Figure 8**. The predicted flow pattern consists of two vortices, with one vortex below the impeller and another above the impeller. The impeller generates a jet stream in the radial direction towards the wall. The flow circulates back to the impeller through the top and lower side of the stator.

Comparisons are made of the measured and predicted mean velocity components  $U_r$ ,  $U_\theta$  and  $U_z$  for the radial, tangential and axial directions respectively. Generally, the agreement is very good between the measured and predicted velocities especially in the axial and radial directions. Different turbulence models and grid refinement have been tested but generally the results remain fairly similar.

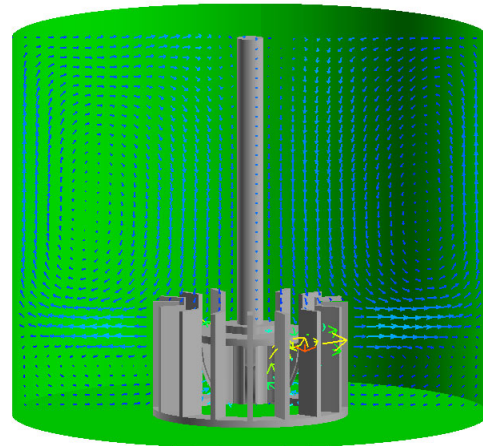


**Figure 8:** CFD predicted velocity vectors in a vertical plane in the Outokumpu flotation cell.

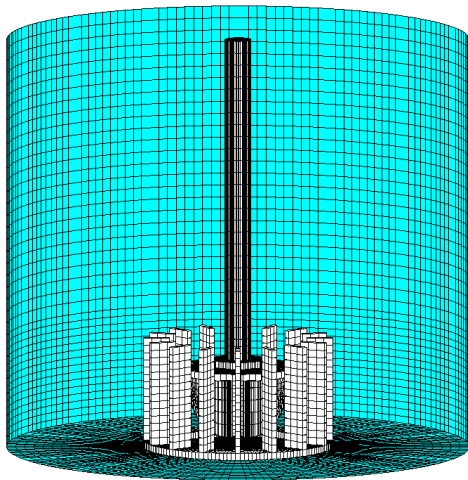


**Figure 6:** Surface grid of the Outokumpu flotation cell.

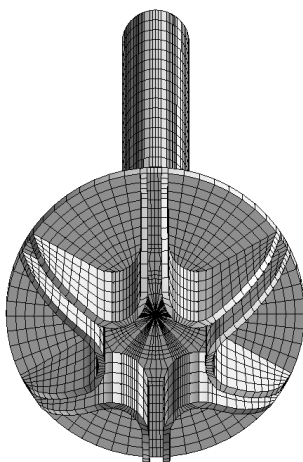


**Figure 7:** Grid of the Outokumpu flotation impeller.

### DISCUSSION

There has been a considerable amount of validation of underlying numerics carried out by CSIRO for the flotation model. The numerical validation work has built on an extensive experience that had been accumulated over several years simulating agitated vessels of various kinds (eg. Koh and Wu, 1998; Lane *et al.*, 1999).

Steady-state simulations have been performed with the multiple-frames-of-reference technique: though it is faster than the transient sliding-mesh method, it has been found to give essentially the same result. When the sliding mesh technique was used, a periodic steady state was achieved after about 20 rotations of the impeller.

More detailed turbulence models have been tested to compare against the  $k-\epsilon$  turbulence model used in this work. For example, the Differential Stress Model for turbulence gave similar results as the  $k-\epsilon$  turbulence model, and did not improve significantly the match between measured and model tangential velocities. It should be pointed out that in real flotation cells, the swirl component is usually damped more than in the ideal water-only experiment due to cell internals or slurry properties.

The flow fields in the cells are strongly inhomogeneous and anisotropic due to the presence of large and strong vortices. In both cases, the turbulence level was the highest near the stator and reduced as the wall or free surface was neared. There are some differences between the measured RMS fluctuating velocities and the predicted turbulence by the model. In the  $k-\epsilon$  turbulence model, individual RMS components are not predicted. But it is possible to sum the measured RMS components and compare it against the value of  $k$  obtained from  $k-\epsilon$  model. It should be noted that the detailed comparison of RMS fluctuations (or equivalently  $k$ ) is complicated by the impeller rotation. The measured values include both the “true” turbulence and the periodic fluctuations in velocity due to the impeller rotation. In principle, it is possible to

synchronise the measurements with a specific phase in the rotation, and so remove the component due to periodic velocity variation, but this is not normally done.

Sensitivity of the model predictions to grid size has also been investigated. It was found that no significant changes in velocity fields were obtained when the number of cells was doubled. Other discretisation schemes (eg. Higher-order upwind, QUICK) have also been tested and found to be no better than the hybrid upwind scheme which allows for second-order central differencing across streams in regions of low flow.

Other investigations have been conducted with air sparging and with solids, and the results will be reported elsewhere: in general the same flow patterns are generally found in the multi-phase cases. From the solution of the flow field, it is possible to characterise the flow in the cells and prevent potential problems such as short-circuiting and solids settling. The power consumption can be estimated from the energy dissipation rate obtained in the simulation. The results will assist in providing suggestions for modifications to the flotation cells.

The models can be utilised to study any design or operational improvements suggested by the flotation cell operators. Individual investigations can involve specific modification to the flotation cells. Numerical modelling is a powerful tool for design, scale-up and optimisation of industrial cells.

## CONCLUSION

The hydrodynamics in two flotation cells fitted with Metso Minerals and Outokumpu flotation mechanisms have been studied using CFD modelling. CFD models provided detailed hydrodynamics of flotation cells that are very useful for progressing knowledge of the flotation. The models are sufficiently accurate for engineering design purposes and so can be used for investigations on the design and operation of flotation cells in parametric studies.

## ACKNOWLEDGEMENT

The authors would like to thank all sponsors of the AMIRA P9M CFD project for permission to publish this paper, and to Metso Minerals and Outokumpu Technology for providing the flotation mechanisms. The authors particularly thank Mr David Stribley of AMIRA International for coordinating the project and his helpful advice.

## REFERENCES

- CFX User Guide, Release 4.4*, (2001) Computational Fluid Dynamics Services, AEA Industrial Technology, Harwell Laboratory, Oxfordshire, UK.
- KOH, P.T.L., MANICKAM M. and SCHWARZ M.P. (2000), "CFD simulation of bubble-particle collisions in mineral flotation cells", *Minerals Engineering*, **13**, 1455-1463.
- KOH, P.T.L. and SCHWARZ M.P. (2003), "CFD modelling of bubble-particle collision rates and efficiencies in a flotation cell", *Minerals Engineering*, **16**, 1055-1059.
- KOH, P.T.L. and WU, J., (1998), "CFD Simulation of Flow in Mechanically Stirred Tanks with Fluidfoil Impellers", *Chemeca 98*, 26th Australasian Chemical Engineering Conference, Port Douglas, September.
- LANE, G., SCHWARZ, M.P. and EVANS, G.M. (1999), "CFD simulation of gas-liquid flow in a stirred tank using a full flow field approach". In *Proc. 3<sup>rd</sup> International Symposium on Mixing in Industrial Processes*, Osaka, Japan, September.
- LAUNDER, B.E. and SPALDING, D.B., (1974) "The numerical computation of turbulent flows", *Comp. Meths. Appl. Mech. Engng.*, **3**, 269-289.
- WILLS, B.A., (1992) "Mineral Processing Technology", 5th Edition, Pergamon Press, Oxford, p. 491-644.

